Journal of Hydroscience and Hydraulic Engineering
Vol. 3, No. 1, April, 1985, pp.1-13.

THREE-DIMENSIONAL FLOW OVER ALTERNATING POINT BARS IN A MEANDERING CHANNEL

BY

Nobuyuki Tamai

Professor, Department of Civil Engineering
University of Tokyo, Tokyo 113, Japan

and

Tsuyoshi Ikeya

Graduate Student, Department of Civil Engineering
University of Tokyo, Tokyo 113, Japan

SYNOPSIS

A mathematical model and experimental results are presented for a flow over alternating point bars in a meandering channel. The mathematical model comprises a transformation of the coordinate and an application of the k-ε model. According to the coordinate transformation, the water body in a unit bend of a meandering channel with bars is transformed into a parallelepiped.

Numerically simulated results are compared with experimental results obtained in a relatively deep flow in a meandering channel. Formation of double cells of secondary flow in a section and bed shear distribution are successfully reproduced by the mathematical model. However, it is said that conventional treatment of the k-ε model is not sufficient to reproduce the details of the sidewall effect in a relatively deeper flow in a meandering channel.

INTRODUCTION

It is scarce to encounter a fairly long straight reach in rivers and a meandering channel seems an essential nature of the longitudinal path of rivers. Strong secondary flows as well as local scour and deposition are observed in a river bend whereupon river engineers have had a keen concern from the standpoint of both flood control and water utilization. Understanding of three-dimensional characteristics of the flow in a meandering channel is needed to completely realize the mechanism of river flow over alternating point shoals in a meandering channel.

Theoretical studies are still far from completion due to mathematical difficulties to treat a fully three-dimensional nature of flow. Existing theories utilize a quasi-three-dimensional approach [Engelund (2), Ikeda et al. (6), Kalkwijk and de Vriend (9), Hasegawa (4), Tamai and Ikeuchi (20), and Tamai and Ikeya (19)]. Fully three-dimensional approach has recourse to numerical simulation. Several attempts have been performed to simulate a three-dimensional flow in a meandering channel by turbulence models [Leschziner and Rodi (12), Demuren (1), Mori and Kishi (13), and Ikeda et al. (7)]. Previous studies, however, are restricted to a rectangular channel or to a fully developed region when an alluvial bed topography is treated.

The method presented herein utilizes a coordinate transformation by which an arbitrary shape of the bed in a meandering channel is expressed by a coordinate surface. A series of experiment was performed in a meandering channel with an idealized shape of alternating point bars. Mean velocity field and the Reynolds stress were measured in a relatively deep flow through a meandering channel.

Computed results by the k-ε model is discussed in comparison with the experimental results.

Majority of the existing experimental studies in a meandering channel were performed for a single bend with a rectangular cross section. Only a few studied velocity distribution in a meandering channel with an alluvial bed. Yen (23), Hasegawa et al. (3), and Tamai and Ali (18) measured water surface profile and longitudinal and lateral components of velocity for an alluvial bed topography in a meandering channel. In the present study measurement of the vertical velocity and the Reynolds stress is also performed in a meandering channel with an idealized shape of alternating point bars to study the three-dimensional flow structure and to calibrate a mathematical model.

This paper is an extended version of the paper published by the authors in Japanese (8).

MATHEMATICAL MODEL

Transformation of Coordinates

In Fig.1 schematic diagrams of the coordinate system, and a perspective of the centerline and a sectional shape of a meandering channel are shown. Here, L = the length of a meander along the centerline, θ = angle between a tangent of the centerline and the direction of the valley axis, and α = angle between the plane on which the channel meanders and the horizontal plane.

The Cartesian coordinate system(y^1, y^2, y^3) is transformed into a general curvilinear coordinate system(x^1, x^2, x^3) so that the water surface, the bottom,

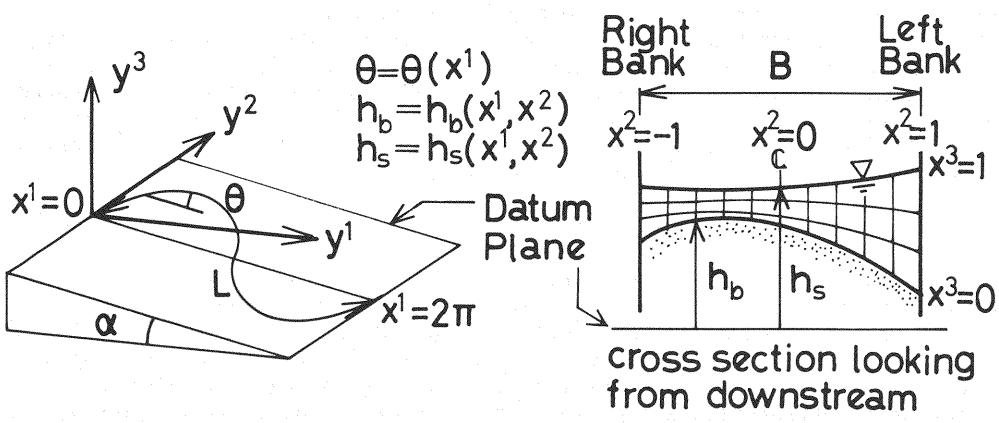

Fig.1 Definition sketch of the coordinates and a meandering channel

and the side walls in a physical domain compose the coordinates surfaces in (x^1, x^2, x^3)-system. This is accomplished by the following transformation.

$$y^1 = \{\int_0^{x^1} \frac{L}{2\pi} \cos\theta dx^1 - \frac{B}{2}x^2\sin\theta\}\cos\alpha + \{(h_s-h_b)x^3 + h_b\}\sin\alpha$$

$$y^2 = \int_0^{x^1} \frac{L}{2\pi} \sin\theta d\,x^1 + \frac{B}{2}x^2\cos\theta \qquad (1)$$

$$y^3 = -\{\int_0^{x^1} \frac{L}{2\pi} \cos\theta dx^1 - \frac{B}{2}x^2\sin\theta\}\sin\alpha + \{(h_s-h_b)x^3 + h_b\}\cos\alpha$$

The metric tensor is given by

$$g_{ij} = \begin{bmatrix} (\frac{L}{2\pi} - \frac{B}{2}x^2\frac{d\theta}{dx^1})^2 + (\frac{\partial z}{\partial x^1})^2, & \frac{\partial z}{\partial x^1}\frac{\partial z}{\partial x^2}, & (h_s-h_b)\frac{\partial z}{\partial x^1} \\ \frac{\partial z}{\partial x^1}\frac{\partial z}{\partial x^2}, & (\frac{B}{2})^2 + (\frac{\partial z}{\partial x^1}), & (h_s-h_b)\frac{\partial z}{\partial x^2} \\ (h_s-h_b)\frac{\partial z}{\partial x^1}, & (h_s-h_b)\frac{\partial z}{\partial x^2}, & (h_s-h_b)^2 \end{bmatrix} \quad (2)$$

where $z = (h_s-h_b)x^3 + h_b$. The determinant of the metric tensor is obtained as in the following equation.

$$g = (\frac{B}{2})^2(\frac{L}{2\pi} - \frac{B}{2}x^2\frac{d\theta}{dx^1})^2(h_s-h_b)^2 \quad (3)$$

Basic Equations

Basic equations for describing the motion of fluid are equation of continuity and the Reynolds equations for incompressible, turbulent flows, such that

$$u^i;\ i = 0 \quad (4)$$

$$u^i;_j u^j = -(Gy^3 + \frac{p}{\rho}),\ ^i - (\overline{u'^i u'^j});_j \quad (5)$$

where u^i = a contravariant component of time-averaged velocity, u'^i = a contravariant component of fluctuating velocity, G = gravitational acceleration, ρ = density, p = pressure, a comma = differentiation, a semicolon = covariant differentiation, and overbar = time averaging process.
Eddy-viscosity concept is applied to express the turbulent stresses, that is,

$$-\overline{u'^i u'^j} = \nu_t(u^i;^j + u^j;^i) - (2/3)\delta^{ij}k \quad (6)$$

where ν_t = scalar eddy viscosity, k = kinetic energy of the fluctuating motion of the flow, and δ^{ij} = the Kronecker delta. Then, Eq.5 is reduced into the following form:

$$(u^i u^j);_j = g^{ji}(-G\partial y^3/\partial x^j - \rho^{-1}\partial p/\partial x^j) + g^{ml}(\nu_t u^i;^l);_m + g^{il}(\nu_t u^m;^l);_m$$
$$- (2/3)g^{ml}\delta^i{}_{lk,m} \quad (7)$$

where g^{ij} = a conjugate of the metric tensor (= cofactor of g_{ij}/g).

Turbulence Model

The eddy viscosity is described by the k-ε model, namely

$$\nu_t = c_\mu\frac{k^2}{\varepsilon} \quad (8)$$

$$(ku^j);_j = (\frac{\nu_t}{\sigma_k}\frac{\partial k}{\partial x^j});_j + \nu_t(u_i;^j + u^j;^i)u^i;_j - \varepsilon \quad (9)$$

$$(\varepsilon u^j);_j = (\frac{\nu_t}{\sigma_\varepsilon}\frac{\partial \varepsilon}{\partial x^j});_j + c_2\frac{\varepsilon}{k}\nu_t(u_i;^j + u^j;^i)u^i;_j - c_2\varepsilon^2/k \quad (10)$$

where ε = the rate of energy dissipation and u_i = a covariant component of a velocity vector. Values of constants in the k-ε model are shown in Table 1 [Rodi (15)].

TABLE 1 VALUES OF THE CONSTANTS IN THE k-ε MODEL

c_μ	c_1	c_2	σ_k	σ_ε
0.09	1.44	1.92	1.0	1.3

Boundary Conditions

Boundary conditons on the bottom and the side walls are expressed by the wall function method. The velocity, the kinematic energy and the energy dissipation at the closest grid to the fixed boundary are given as follows:

$$\begin{cases} \dfrac{U}{u_*} = \dfrac{1}{\kappa}\ln\dfrac{y}{k_s} + A_r \\ k = u_*{}^2/\sqrt{c_\mu}, \quad \varepsilon = u_*{}^3/\kappa y \end{cases} \tag{11}$$

where U = the magnitude of the tangential component of velocity to the wall, k_s = roughness height, A_r = constant, κ = Karman constant, u_* = shear velocity ($=\sqrt{\tau/\rho}$), y = distance from the wall, and τ = the tangential component of stress exerting on the wall.

Following conditions are imposed at the water surface.

$$\begin{cases} p = 0, \; u^3 = 0, \; \nu_t u^1{}_{;3} = 0, \; \nu_t u^2{}_{;3} = 0 \\ k_{,3} = 0, \; \varepsilon_{,3} = 0 \end{cases} \tag{12}$$

In the present computing process the water surface elevation is adjusted so as to satisfy the condition p = 0 at the water surface.

At the entrance and the outlet of one unit bend of a meandering channel it is assumed that the same hydraulic conditions are established repeatedly. This condition corresponds to uniform flow in open channels and the normal depth of uniform flow is also obtained through simulation.

Solution Procedure

Basic assumption to solve the set of relations through Eq.4 to Eq.10 is that no flow reversal occurs in the longitudinal direction. Therefore, partial derivatives and covariant derivatives with respect to x^1 are neglected in the process of descretization (12). For the finite difference representation of advection terms QUICK [Leonald (11)] is utilized. Other procedures follow the same line described in Demuren (1).

EXPERIMENTAL PROCEDURES AND RESULTS

Experimental Set-Up and Procedures

An outline of experimental flume and symbols for the coordinate are shown in Fig.2. Planimetric shape of the flume is similar to that utilized by Kinoshita (10) for the similarity law of a meandering where the centerline of the flume follows a sine-generated curve. The maximum deviation angle between the tangent of the centerline and the meandering belt is 20 degrees, wave length of a meander is 160cm, and the width of the flume is 20cm. The bed slope in the

direction of the meandering belt is 1/1000. An idealized shape described subsequently is adopted for alternating point bars. The variation of the bed level from a uniformly sloping plane in the direction

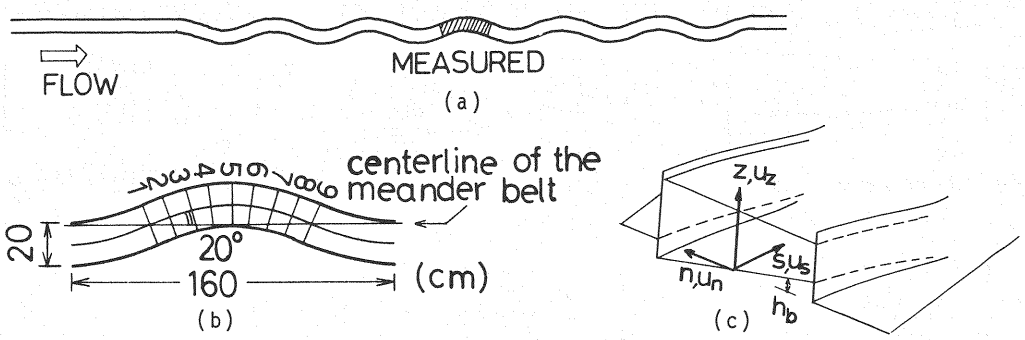

Fig.2 (a) Plan of the experimental flume, (b) Location map of the section (c) Coordinate system and symbols.

of the meandering belt is explained by $h_b = -(2n/B)\sin(2\pi s/L)$ in cm unit where L is the meander length along the centerline and the origin of s-coordinate is taken at section 1 shown in Fig.2(b). The bed of the flume is molded by cement mortar and painted on the surface. Vertical side walls are constructed by a plastic plate.

Discharge rate was determined so as to produce the same water depth at the entrance and the exit sections of a unit bend, and discharge of 3ℓ/s satisfied the required condition. The measuring section was chosen in the middle reach of the flume (shaded area in Fig.2(a)) in order to avoid upstream and downstream effects. Average water depth over a unit bend was 5.2cm. Measurement of water level was performed by a point gage at 9 sections shown in Fig.2(b). Lateral interval of the measuring point was 2cm. Velocity measurements were done by a hot-film anemometry with a split-type dual component sensor. The number of measuring points for three components of the velocity was between 54 and 58 in one section and nine sections in the longitudinal direction, which amounted to 505 points for a unit bend. To obtain the three components of the velocity the measurement was repeated three times at one point setting a dual component sensor in the longitudinal vertical plane, in the horizontal plane and in an oblique plane which passes the intersection of the longitudinal and the horizontal plane with the angle of 45 degrees to the horizontal plane. Signals of the hot-film anemometer were recorded by a tape recorder and were discretized by an A-D converter. Sampling frequency was 100 Hz and sampling time was 30 seconds.

Experimental Results and Discussion

Measured isovels and contours of Reynolds stress components at representative sections are shown in Fig.3. Fig.3(a) shows the isovels of the primary velocity where at the section 1 higher velocity core is observed in the middle third in lower half of the depth and in the second quarter from the concave bank in the upper half of the depth. In the middle part of the depth in the section 1,

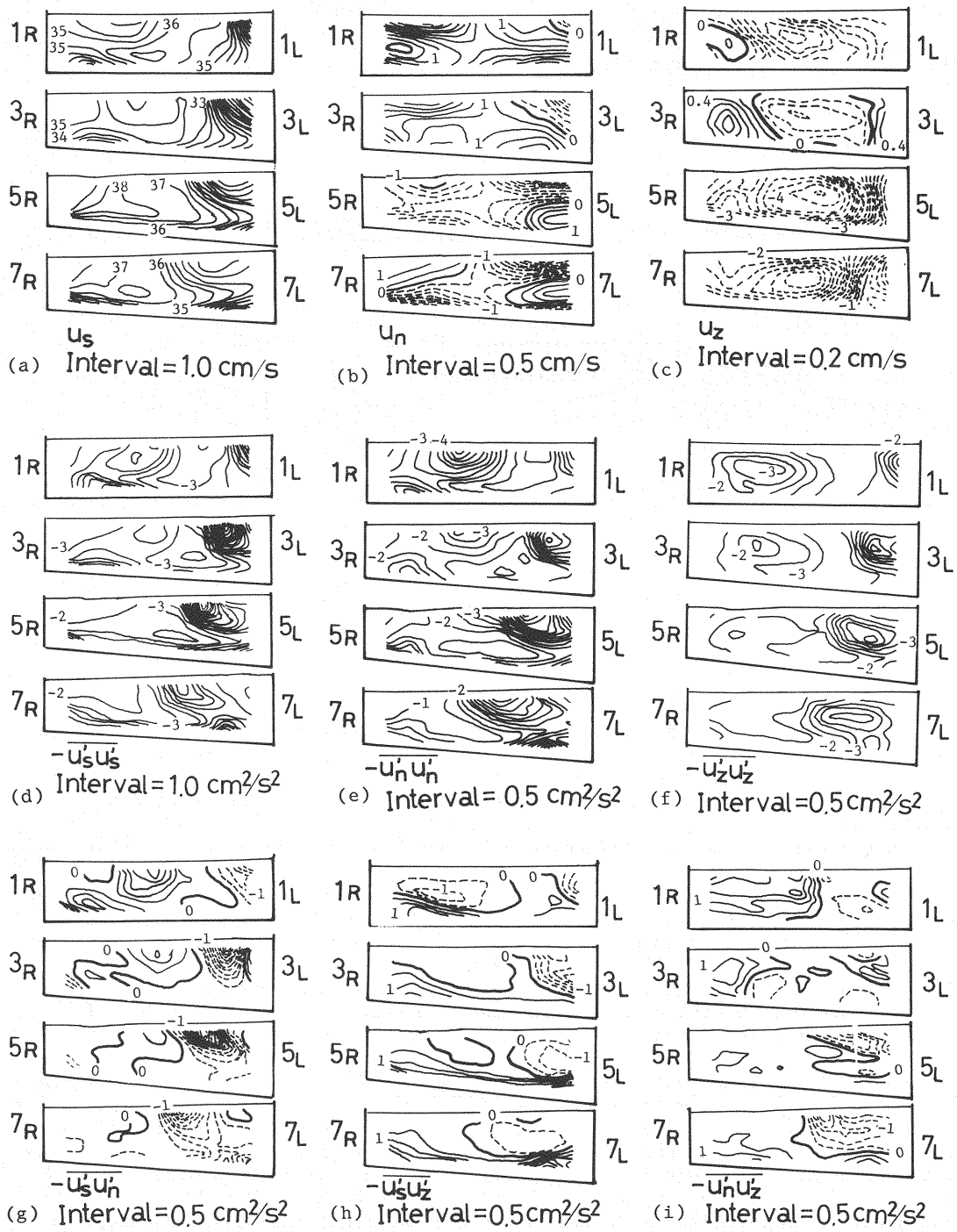

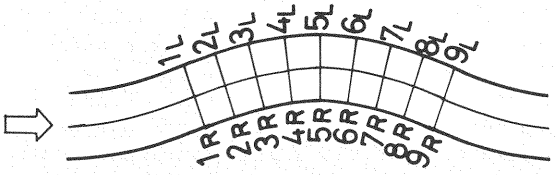

Fig.3 Contours of observed mean velocity and Reynolds stresses and a location map of the section

a higher velocity core extends to the convex bank. At the section 3 which corresponds to upper one quarter in the longitudinal direction, a fairly uniform velocity distribution is observed, though higher velocity is seen near the water surface along the convex bank. At the apex of a unit bend a higher velocity core covers a fairly large part of the section from the central part toward a region close to the convex bank. At the section 7 where the distance from the entrance is three quarters of a unit bend a higher velocity core appears in the right half section of the convex bank side. The longitudinal transition of a higher velocity core is similar to that observed in a meandering channel with a rectangular section [Rozovskii (16), Tamai et al. (17)]. This is because the experiment was performed for a relatively deep flow, for which the width to depth ratio is about four and the height of alternating bars was not so large. As for the vertical distribution of the local primary velocity, it is found that the maximum appears in the middle of the water depth at many locations. That is also one of typical features of the flow in a meandering channel with a flat fixed bed [Yen (22), Tamai et al. (17)].

Fig.3(b) shows the isovels of the lateral velocity component of the time-averaged velocity where the broken lines indicate the minus sign, that is, flow toward the convex bank. The solid lines indicate flow toward the concave bank. The density of the isovels seems to increase in the latter half of a unit bend. In the downstream half of a unit bend, the lateral component directs toward the concave bank in the middle part of the depth and toward the convex bank both near the surface and near the bottom in a half section near the concave bank side. In the region near the convex bank, the lateral velocity directs toward the concave bank near the surface and toward the convex bank near the bottom. In the entrance region of a unit bend the direction of lateral component tends to be reversed, which shows the effect of a preceding bend still remains in the upstream region of a unit bend.

The vertical component of velocity is shown in Fig.3(c) where the direction is positive upward. The density of isovels begins to increase in the downstream half of a unit bend. Large magnitude of the downward velocity illustrated in sections 5 and 7 are attributed to the deviation of the setting angle of a sensor in case of measurement. Because the distribution of the primary velocity is approximately uniform in the large part over a unit bend, the shift of small constant velocity caused by the oblique setting does not produce large torsion in the velocity vector.

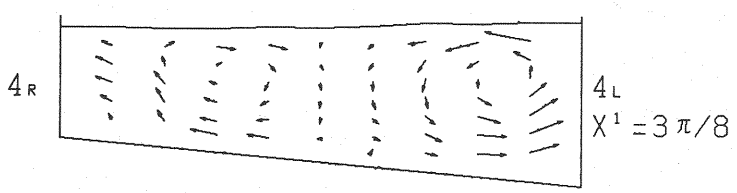

Fig.4 Observed secondary velocity vector in the section 4

From the data of the lateral and the vertical components, local velocity vectors in a section is constructed as in Fig.4. Considering the fact that the setting of a probe might deviate from the idealized position and angle, residual from the sectional mean of the lateral and vertical components were utilized to construct a local velocity vector. In this figure two countering cells are found, which is a typical feature in a mid-part of the longitudinal path of a unit bend in a meandering channel both in laboratory experiments and in field

observation [Yen (22), Yen (23), Kinoshita (10), Tamai et al. (17), and Thorne and Hey (21)]. The two cells in Fig.4 look as if they separate the section into two compartments by a vertical sector at the center. On this point the shape of circulating cells differs from reported patterns in previous papers where combination of a residual top cell and a developing secondary cell along the bottom was seen. The discrepancy of the cell pattern from the existing result may be attributed to the less accuracy in setting of a probe.

Hereafter, the distribution of the correlation of turbulence velocity is explained. When the density of water ρ is multiplied, these correlation comprise six components of the Reynolds stress which determine the whole component of a symmetric tensor. A zone of large absolute value of $-u_s'u_s'$ and $-u_n'u_n'$ is seen near the water surface of the concave bank side of the section in the entrance region of a unit bend and thereafter it extends toward the central part of the section near the apex of the bend. In the convex bank side of the section absolute value of $-u_s'u_s'$ and $-u_n'u_n'$ is large near the bottom and small near the water surface. The distribution of $-u_z'u_z'$ shows the similar pattern to other diagonal components of a correlation tensor of the turbulent velocity, though the large absolute value appears below the water surface. This is supposed that the existence of the water surface suppressed the vertical component of turbulence near the water surface.

The value of $-u_s'u_n'$ shows a similar distribution to that of $-u_n'u_n'$ and is negative in the surface region near the concave bank. The zone of negative $-u_s'u_n'$ extends to the corner composed of the bottom and the concave bank wall. The value of $-u_s'u_z'$ becomes positive near the bottom and negative in the surface region near the concave bank. This component corresponds to the shear stress substantially determined by the vertical gradient of the velocity vector. The distribution of the plus and minus signs of $-u_s'u_z'$ roughly agrees with that of the vertical gradient of the primary velocity u_s. Although accuracy of the present measurement of $-u_n'u_z'$ is considered not so high, $-u_n'u_z'$ takes positive value in the bottom region near the side walls and negative value in the surface region near the concave bank side. Like the average velocity field, the remaining effect of a preceding bend is also seen in sectional distribution of the quadratic correlation of turbulent veloity components.

COMPUTED RESULTS AND COMPARISON WITH EXPERIMENTAL RESULTS

Specified conditions for computation were the same as those experienced in the flume experiment aforementioned. Numbers of mesh points utilized in a unit bend are 32, 20, and 10 in x^1, x^2, and x^3 directions, respectively.

Time-Averaged Velocity Field

Fig.5 shows isovels of the physical components of average velocity in the transformed curvilinear coordinate. Although the transverse direction perpendicular to the side wall does not coincide with coordinate line of x^3 = const. from rigorous point of view, $\tilde{u}^2$ is approximately regarded as u_n.

Higher velocity core of the primary velocity (Figs.3(a) and 5(a)) which exists at the center in the entrance region of a unit bend moves toward convex bank near the water surface and the maximum velocity along one vertical line appears in the mid-part of the water depth near concave bank. Computed results reproduce this tendency. However, coincidence of the pattern of the predicted isovels with the measured ones is relatively poor. It is supposed that the k-ε model is not sufficient to take the influential effect of the water surface on the Reynolds stress into account in case that width to depth ratio of the flow is small like in a present case ($\cong$4).

Secondary Circulations

Secondary flow patterns can be reprocuded fairly well by the computation

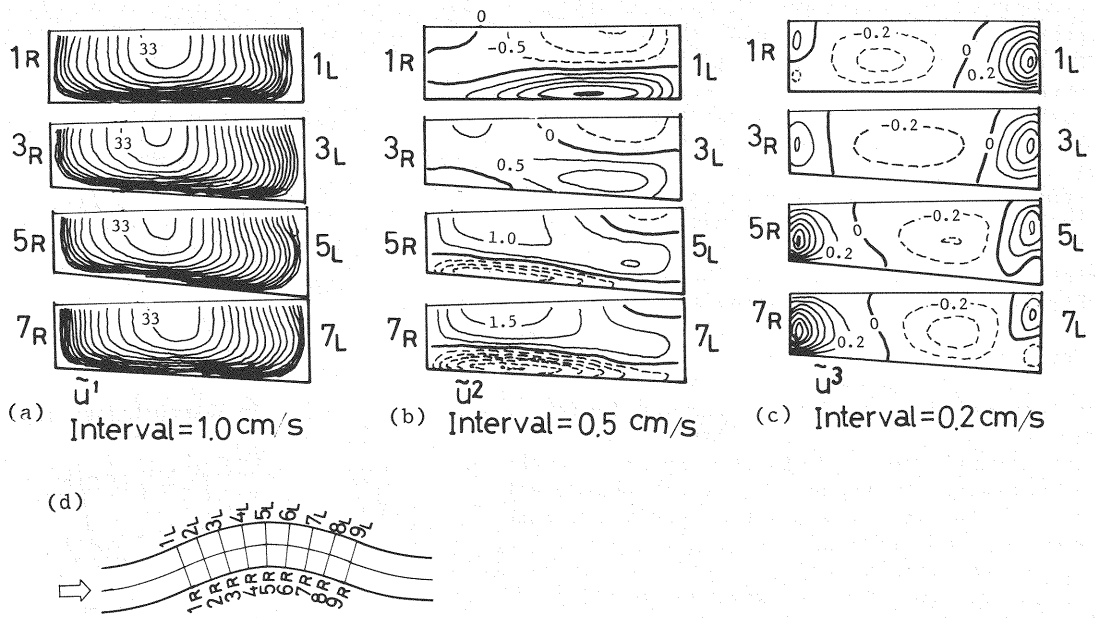

Fig.5 Isovels of simulated mean velocity and a location map of the section

both in transverse and vertical directions. Large values for the vertical component in sections 5 and 7 are caused by deviation of the setting angle of a sensor in case of measurement. Because the distribution of the primary velocity is approximately uniform in the larger part through bend, the shift of constant velocity caused by this oblique setting does not affect much on the results of other hydraulic quantities.

Fig.6 shows predicted velocity-vector distribution in the section 4. Two cells are seen in this figure as described previously. The top cell is a residual one generated in the preceding bend and the bottom cell is a developing secondary circulation in the present bend. This result may be the first simulation that reproduces the double-cell pattern of the secondary flow. However, there is still incompleteness in the simulation for the detailed features.

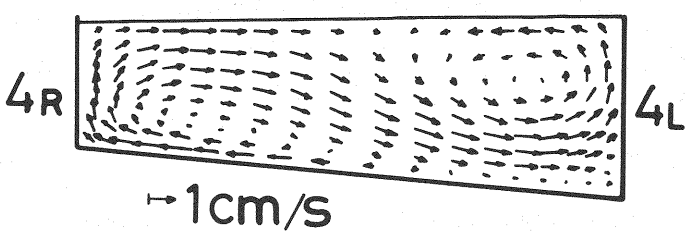

Fig.6 Predicted secondary velocity vector in the section 4

Bed Shear Distribution and the Eddy Viscosity

As an example of turbulence quantities bed shear distribution obtained in the simulation is shown in Fig.7. In Fig.7 broken lines indicate traces of the location where the average shear over a unit bend appears. High shear stress region, where shear stress exceeds the bend average, appears near a convex bank at the entrance of a unit bend. It remains near a convex bank side in the

upstream half of a unit bend. Then the high shear stress region begins to migrate toward a concave bank after the flow passes the apex of a unit bend. The variation of the bed shear obtained in the simulation agrees qualitatively with existing data published by Yen (22) for a trapezoidal section and Yen (23) and Hooke (5) for an equilibrium alluvial bed. The transverse migration of the high shear zone is more distinct in case of an equilibrium alluvial bed where a deep scour hole along a concave bank generates the convergence of large amount of water mass toward a concave bank.

Back to Fig.3 (a), it is noted that the pattern of isovels of the primary velocity is much more complex than that estimated by a mathematical model. Velocity profiles in the vertical and the transverse directions do not change monotonously and are strongly deformed from those observed in a straight channel. As for the vertical velocity profile, a 'so-called' barrel type in which the maximum velocity appears far below the water surface is observed at nearly all locations in the downstream half of a unit bend. The stronger intrusion of higher isovels into a concave bank in the middle of the water depth is obvious in the measured results. Furthermore, the vertical gradient of isovels seems to be kept considerably large near the water surface in the measurement. Therefore, it is suggested that the boundary condition of the shear stress at the water surface may have to be revised as well as the turbulence model in order to predict the flow behavior in a relatively deep flow in a meandering channel [Naot and Rodi (14)].

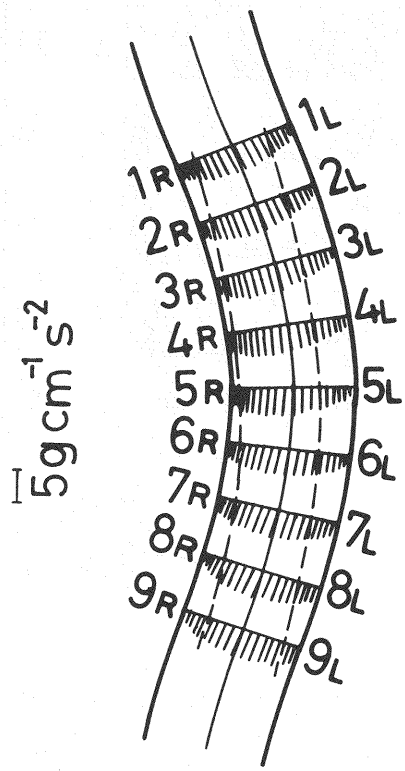

Fig.7 Bed shear distribution

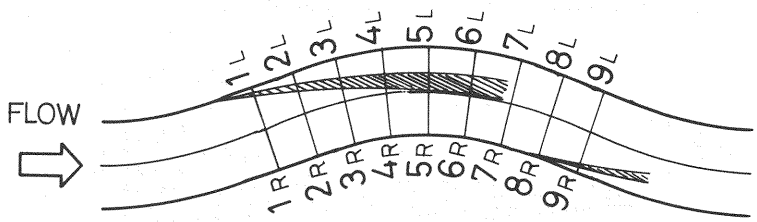

Fig.8 Observed eddies on the water surface

In Fig.8 the shaded areas show the rigions where eddies were observed on the water surface. In these regions large values of correlations of turbulence velocity in the longitudinal and the transverse directions were also observed near the water surface. It is revealed that higher degree of approximation than that used in the k-ε model for the turbulence quantity is needed in these areas.

Fig.9 shows the distribution of the eddy viscosity in several sections. The maximum value in a section appears at the water surface and the transverse location of this sectional maximum seems to follow the same longitucinal trail as the migration of the higher bed shear zone. The maximum value of ν_t in one unit bend is observed at the water surface in a little downstream section from the apex of one unit bend. The distribution of ν_t in the bottom half of the water depth remains unchanged through a unit bend in a meandering channel. In

a theory developed by Tamai and Ikeya (19) the following function is adopted for ν_t.

$$\nu_t = \begin{cases} (\kappa u_* h/4)\eta(1-\eta) & \text{for } 0 \leqq \eta \leqq 0.5 \\ \kappa u_* h/4 & \text{for } 0.5 \leqq \eta \leqq 1 \end{cases} \quad (13)$$

where $\eta = z/h$ and h is the local water depth. The trend of vertical variation of ν_t follows (13) up to $\eta = 0.5$, but Fig. 9 reveals that the value of ν_t continues to increase toward the water surface. Therefore, the simulated result will provide the means of improvement for a theoretical approach. An experimental determination of the eddy viscosity was not achieved because of the difficulty to perform numerical differentiation for velocity data. More precise and detailed measurements are needed to obtain the experimental data of ν_t.

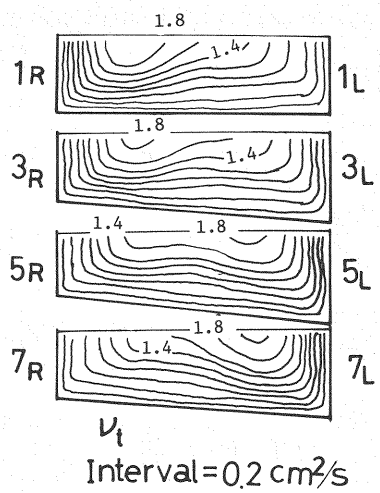

Fig.9 Distribution of the eddy viscosity

CONCLUDING REMARKS

Conclusions obtained in this study are summarized as below.

1) A mathematical model is developed for the flow with alternating point bars in a meandering channel. The double-cell pattern of the secondary flow is reproduced by the present mathematical simulation.
2) Simulation of isovels of the primary velocity indicates that the combination of the k-ε model with conventional treatment of the shear stress at the water surface is not sufficient for the flow in a meandering channel in case that the width to depth ratio is small.
3) Distribution of the bed shear stress is reproduced qualitatively by the k-ε model for the flow over alternating bars in a meandering channel. In this context a new technique to measure the bed shear exerting on complex three-dimensional bar surface is needed to test the theory procisely.
4) Although global features of the flow over alternating bars in a meandering channel are reproduced by the k-ε model, future revision is still needed to trace the detailed behavior of a three-dimensional flow under complex boundaries.

ACKNOWLEDGEMENT

A part of this study was supported by the Grant-in-Aid(59020003, Representative of the research group is Prof. T. Kishi, Hokkaido Univ.) of the Ministry of Education, Science, and Culture of Japan.

REFERENCES

1. Demuren, A.O. : Three dimensional numerical computation of flow and pollutant dispersion in meandering channels, Proc.20th Congress, IAHR, Vol.III, pp.29-46, 1983.
2. Engelund, F. : Flow and bed topography in channel bends, Proc.ASCE, Vol.100, HY11, pp.1631-1647, 1974.
3. Hasegawa, K., I. Yamaoka, Y. Watanabe and S. Sasajima : Theory and experiments on the flow over alternating bars in a strongly curved channel, Proc. Hokkaido Section, Japan Soc. Civil Engineers, pp.191-196, 1982(in Japanese).
4. Hasegawa, K. : A study on flow and bed topographies in meandering channels, Proc.JSCE, No.338, pp.105-114, 1983(in Japanese).
5. Hooke, R.L. : Shear-stress and sediment distribution in a meander bend, UNGI-report 30, Univ. of Uppsala, 58p., 1974.

6. Ikeda, S., M. Hino and H. Kikkawa : Theoretical study on the free meandering of rivers, Proc.JSCE, No.255, II-2, pp.63-73, 1976(in Japanese).
7. Ikeda, S., M. Tanaka and M. Chiyoda : Characteristics of turbulent flow in a meandering air duct, Proc.JSCE, No.351, II-2, pp.77-86, 1984(in Japanese).
8. Ikeya, T. and N. Tamai : Three-dimensional flow over alternating bars in meandering channels, Proc.29th Japanese Conf. on Hydraulics, JSCE, pp.697-702, 1985(in Japanese).
9. Kalkwijk, J.P.Th. and H.J. de Vriend : Computation of the flow in shallow river bends, J. Hyd. Research, IAHR, Vol.18, No.4, pp.327-342, 1980.
10. Kinoshita, R. : Similarity law on a meandering channels of a mild slope three-dimensional experiment, The Ishikari River Construction Bureau, 164p., 1974(in Japanese).
11. Leonald, B.P. : A stable and accurate convective modelling procedure based on quadratic upstream interpolation, Comp. Mech. Appl. Mech. Eng., Vol.19, pp. 59-98, 1979.
12. Leschziner, M.A. and Rodi, W. : Calculation of strongly curved open channel flow, Proc.ASCE, Vol.105, HY10, pp.1297-1314, 1979.
13. Mori, A. and T. Kishi : A study on the secondary flow in open channel bend with transverse sloping bed, Proc.28th. Japanese Conf. on Hydraulics, JSCE, pp.751-755, 1984(in Japanese).
14. Naot, D. and W. Rodi : Calculation of secondary currents in channel flow, Proc. ASCE, Vol.108, HY8, pp.948-968, 1982.
15. Rodi, W. : Turbulence Models and Their Application in Hydraulics, STATE-OF THE-ART-PAPER, IAHR, p.29, 1980.
16. Rozovskii, I.L. : Flow of Water in Bends of Open Channels, Israel Program for Scientific Transrations, 233p., 1961.
17. Tamai, N., K. Ikeuchi, A. Yamazaki and Ali A. Mohamed : Experimental analysis on the open channel flow in rectangular continuous bends, J. Hydrosci. and Hydraulic Eng., JSCE, Vol.1, No.2, pp.17-31, 1983.
18. Tamai, N. and Ali A. Mohamed : Velocity profiles in rectangular continuous bends with alluvial bed, Proc.38th Annual Meeting, JSCE, pp.585-586, 1983.
19. Tamai, N. and T. Ikeya : An analytical three-dimensional approach to the flow in rectangular meandering channels, Proc. 4th Congress, Asian and Pacific Regional Div., IAHR, Vol.1, pp.831-845, 1984.
20. Tamai, N. and K. Ikeuchi : Longitudinal and transverse variations of the depth-averaged flow fields in a meandering channel, J. Hydrosci. and Hydraulic Eng., JSCE, Vol.2, No.2, pp.11-33, 1984.
21. Thorne, C.R. and R.D. Hey : Direct measurements of secondary currents at a river inflexion point, Nature, Vol.280, pp.226-228, 1979.
22. Yen, B.C. : Characteristics of subcritical flow in a meandering channel, Inst. of Hydraulic Research, Univ. of Iowa, 77p., 1965.
23. Yen, C.L. : Bed topography effect on flow in a meander, Proc.ASCE, Vol.96, HY1, pp.57-73, 1970.

APPENDIX-NOTATION

The following symbols are used in this paper:

A_r = constant in the logarithmic velocity distribution;

B = width of a channel;

c_μ, c_1, c_2 = constants in the k-ε model;

G = gravitational acceleration;

g_{ij} = metric tensor;

g = determinant of the metric tensor;

h_b = elevation of the bed surface from the datum line;

h_s = elevation of the water surface from the datum line;

k = kinetic energy of the fluctuating motion of flow;

k_s = roughness height;

L = length of a meander measured along the centerline;

n = coordinate axis perpendicular to the centerline of a meandering channel;

p = pressure;

s = coordinate axis tangent to the centerline of a meandering channel;

U = tangential component of velocity to the wall;

$u*$ = local shear velocity;

u_s, u_n, u_z = velocity components in s, n and z directions, respectively;

u^i, u_i = contravariant and covariant component of a velocity vector;

u'^i = contravariant component of fluctuating velocity;

x^1, x^2, x^3 = coordinate axes in a general curvilinear coordinate system; x^1 is taken along the centerline, x^2 perpendicular to the centerline, and x^3 in the vertical direction;

y = local distance from the wall;

y^1, y^2, y^3 = Cartesian coordinate system (see Fig.1);

z = vertical coordinate axis;

comma = differentiation;

overbar = time averaging process;

semicolon = covariant differentiation;

α = angle between the plane on which the channel meanders and the horizontal plane;

δ^{ij} = Kronecker's delta;

ε = rate of energy dissipation;

θ = angle between a tangent of the centerline and the direction of the valley axis;

κ = Karman constant;

ν_t = scalar eddy viscosity;

ρ = density of water;

σ_k, σ_ε = constants in the k-ε model; and

τ = tangential component of stress exerting on the wall.